Vol 17 No 3, March 2008
1674-1056/2008/17(03)/1000-08

Chinese Physics B

© 2008 Chin. Phys. Soc.
and IOP Publishing Ltd

Towards 640 Gbit/s wavelength conversion based on nonlinear polarization rotation in a semiconductor optical amplifier*

Feng Chuan-Fen(冯传奋)†, Wu Jian(伍 剑), Zhang Jun-Yi(张君毅), Xu Kun(徐 坤), and Lin Jin-Tong(林金桐)

The Key Laboratory of Optical Communication and Lightwave Technologies of MOE, Beijing University of Posts and Telecommunications, Beijing 100876, *China*

(Received 10 March 2007; revised manuscript received 28 August 2007)

Taking into account ultra-fast carrier dynamics, this paper models 640 Gbit/s wavelength conversion scheme based on nonlinear polarization rotation (NPR) in a single semiconductor optical amplifier (SOA) and investigates the performance of this kind of wavelength conversion scheme in detail. In this model, two carrier temperature equations are introduced to substitute two energy density equations, which reduce the complexity of calculation in comparison with the previous model. The temporary gain and phase shift dynamics induced by ultra-short optical pulses are numerically simulated and the simulated results are qualitatively in good agreement with reported experimental results. Simulated results show that non-inverted and inverted 640 Gbit/s wavelength conversions based on NPR are achieved with clear open eye diagrams. To further investigate the performance of the non-inverted wavelength conversion scheme, the dependence of output extinction ratio (ER) on some key parameters used in simulation is illustrated. Furthermore, simulated analyses show that high performance non-inverted wavelength conversion based on NPR can be achieved by using a red-shifted filtering scheme.

Keywords: all-optical wavelength conversion, nonlinear polarization rotation, semiconductor optical amplifier, ultra-fast carrier dynamics

PACC: 4265K, 4225J, 4255P

1. Introduction

In the optical networks, all-optical wavelength conversion is one of the key functions for wavelength reuse and non-blocking wavelength routing. Extensive research has been dedicated to semiconductor optical amplifier (SOA) based wavelength conversions due to their power efficiency and integration potential. Several wavelength conversion techniques have been demonstrated by exploiting nonlinear mechanism in SOAs including cross-gain modulation (XGM),[1,2] cross-phase modulation (XPM)[3] and four-wave mixing (FWM).[4] Each scheme has its own advantages and disadvantages. For example, wavelength conversion utilizing FWM in a SOA is independent of the modulation format but it has low conversion efficiency and also the input signal needs to be polarization matched.[5] Wavelength conversion based on XGM in a single SOA has been demonstrated at 100 Gbit/s, but this scheme leads to a degradation of extinction ratio (ER).[6] Wavelength conversion based on XPM in combination with XGM in SOA leads to an improved ER, but this scheme needs two SOAs and the conversion speed of XGM and XPM are limited by the carrier's recovery time.[7] This sets a limit to the maximum operation speed of the wavelength conversion.

Recently, wavelength conversion based on nonlinear polarization rotation (NPR) is received tremendous research efforts.[8,9] A clear advantage of the wavelength conversion based on NPR is that it allows inverted and non-inverted wavelength conversions as well as reshaping using a single SOA.[8] Furthermore, there is a remarkable similarity between the characteristics of a wavelength conversion based on NPR in a single SOA and wavelength conversion based on XPM,[8] which leads to an improved ER with a single SOA. Most of the research work on wavelength conversion based on NPR has focused on tens of gigabits per second rate driven by inter-band transitions. However, the response time of these nonlinearities is restricted

*Project supported by the Ministry of Education of China (Grant Nos 105036 and NCET-04-0116).

†E-mail: fengchuanfen@gmail.com

by the electron–hole recombination time, typically a few hundred picoseconds.[10] This response time fundamentally limits the speed of wavelength conversion that is driven by inter-band transitions.

In this paper, we investigate the probability of wavelength conversion based on NPR at the rate of 640 Gbit/s and discuss the performance of the non-inverted wavelength conversion scheme in detail. Firstly, a model of wavelength conversion based on NPR, which takes into account ultra-fast carrier dynamics, is developed in Section 2. In Section 3, we will present simulated results which reveal temporary characteristics induced by ultra-short optical pulses with different polarization modes and simulated results of the non-inverted and inverted wavelength conversions based on NPR at 640 Gbit/s. The output ER of the non-inverted wavelength conversion as the function of some key parameters is also discussed. Furthermore, a kind of high performance non-inverted wavelength conversion based on NPR assisted with red-shifted filtering scheme is also presented. Finally, the paper is summarized in Section 4.

2. Working principle and numerical model

The configuration of all-optical wavelength conversion based on NPR is illustrated in Fig.1(a). The polarization states of the output probe signals from the polarization controller PC3 for non-inverted wavelength conversion are shown in Fig.1(b). When no pump signal is injected into SOA, the output polarization state of probe signal is perpendicular to the principal axis of PBS by adjusting polarization controllers, thus the probe signal is forbidden to go out of PBS. When pump signal is injected into SOA, the injected pump signal introduces additional birefringence in the SOA, which causes the TE and the TM modes of the probe signal to experience a different refractive index. As a consequence, the output polarization state of the probe signal is rotated about 90° with a proper pump power, thus the probe signal is permitted to go out of PBS. Hence, the increase in the intensity of the pump signal leads to the increase in the intensity of the probe signal that outputs through the PBS. In this way, the non-inverted wavelength conversion from pump signal wavelength to probe signal wavelength can be achieved.

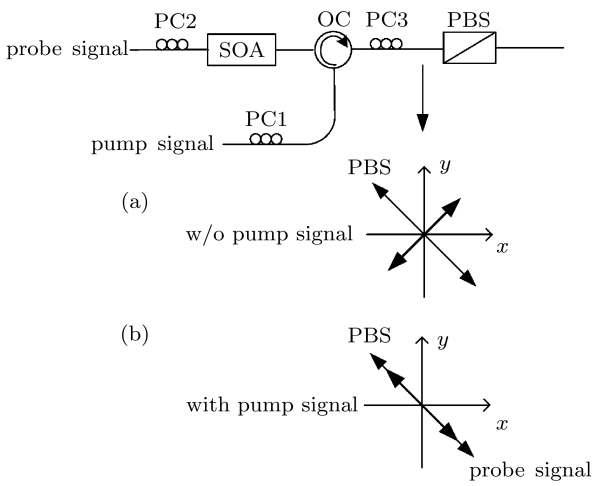


Fig.1. Principle of all-optical wavelength conversion based on NPR. OC: optical circulator; PBS: polarization beam splitter; PC: polarization controller.

In the same way, the polarization controllers can also be adjusted so that initially a maximum amount of probe signal can pass through the PBS. If a saturating pump signal is applied, the phase change between the TE and TM modes leads to a lower intensity at the PBS output. Thus, the increase in the pump intensity leads to the decrease in the probe intensity at the PBS output. In this way, the inverted wavelength conversion is realized.

The model of NPR induced by ultra-short optical pulses in a SOA is based on Ref.[11], except that we introduce two carrier temperature equations to substitute two energy density equations to reduce the complexity of calculation, which can be derived from the rate equations for the carrier density and energy density.[12] The propagation equations, carrier density equations and gain equations for TE/TM modes can be obtained from Ref.[11]. The extensive description will not be repeated here.

The temperature $T_{\rm c}(z,\tau)$ in the conduction band (CB) and the temperature $T_{\rm v}(z,\tau)$ in the valence band (VB) satisfy:

$$\begin{aligned}\frac{\partial T_i(z,t)}{\partial t} &= h_i[u_i - E_i]v_{\rm g}\Big[g^{\rm TE}(z,t)S_0^{\rm TE}(z,t)\\ &\quad +g^{\rm TM}(z,t)S_0^{\rm TM}(z,t)\Big]\\ &\quad +h_i\beta_i\hbar\omega_0 n_i v_{\rm g}\Big[S_0^{\rm TE}(z,t)\\ &\quad +S_0^{\rm TM}(z,t)\Big] - \frac{T_i(z,t)-T_{\rm L}}{\tau_{\rm hi}}\\ &\quad +h_i[E_{2i}-u_i]v_{\rm g}\beta_2\Big[S_0^{\rm TE}(z,t)\\ &\quad +S_0^{\rm TM}(z,t)\Big]^2, \end{aligned} \tag{1}$$

where, i = c, v. Equation (1) for the carrier temperatures $T_i(z,\tau)$ is derived from the rate equations given in Ref.[11] for the energy densities $U_i(z,\tau)$ by expansion, $U_i \cong U_i(N_\mathrm{b}, T_\mathrm{L}) + \mu_i(N - N_\mathrm{b}) + h_i^{-1}(T_i - T_\mathrm{L})$, where N_b is related to the injection current I through the carrier rate equation for N with $S_0^{\mathrm{TE/TM}} = 0$. It is a good approximation for pulses much shorter than the carrier lifetime.[12] Thus, $u_i = (\partial U_i/\partial N)_{T_i}$ and $h_i^{-1} = (\partial U_i/\partial T_i)_N$, which are calculated from the expressions for $U_i(z,\tau)$. The other parameters in Eq.(1) are: group velocity v_g, gains for TE/TM modes $g^{\mathrm{TE/TM}}(z,\tau)$, photo densities for TE/TM modes $S_0^{\mathrm{TE/TM}}(z,t)$, free carrier absorption (FCA) coefficients β_i, carrier densities n_i, two-photon absorption (TPA) coefficient β_2, corresponding carrier energies E_i and E_{2i} (positive, measured from respective band edges), temperature relaxation times τ_{hi}, and T_L is the lattice temperature.

The total electron density $N(z,\tau)$, the temperature $T_\mathrm{c}(z,\tau)$ in the CB and the hole density $P(z,\tau)$, the temperature $T_\mathrm{v}(z,\tau)$ in the VB are needed to calculate self-consistently in each time-step with the quasi-Fermi level $E_\mathrm{fc}(z,\tau)$ of the electrons and the quasi-Fermi level $E_\mathrm{fv}(z,\tau)$ of the holes, using

$$N(z,\tau) = \int \rho_\mathrm{c}(E) F(E_\mathrm{fc}, T_\mathrm{c}, E)\mathrm{d}E, \tag{2}$$

$$P(z,\tau) = \int \rho_\mathrm{v}(E)\left[1 - F(E_\mathrm{fv}, T_\mathrm{v}, E)\right]\mathrm{d}E, \tag{3}$$

where ρ_c and ρ_v are the state densities in the CB and VB, $F(\mu, T, E)$ is the Fermi–Dirac distribution function. The Fermi–Dirac distribution function defined as

$$F(\mu, T, E) = 1 \Big/ \left[1 + \exp\left(\frac{E-\mu}{k_\mathrm{B}T}\right)\right], \tag{4}$$

where k_B is the Boltzmann constant.

The quasi-Fermi level E_fc in the CB and the quasi-Fermi level E_fv in the VB can be estimated using the Nilsson approximation,[13]

$$\begin{aligned} E_\mathrm{fc} &= E_{\mathrm{c}0} + \left\{\ln\delta + \delta[64 + 0.05524\delta(64+\sqrt{\delta})]^{-\frac{1}{4}}\right\} \\ &\quad \times k_\mathrm{B}T_\mathrm{c}, \end{aligned} \tag{5}$$

$$\begin{aligned} E_\mathrm{fv} &= E_{\mathrm{v}0} - \left\{\ln\varepsilon + \varepsilon[64 + 0.05524\varepsilon(64+\sqrt{\varepsilon})]^{-\frac{1}{4}}\right\} \\ &\quad \times k_\mathrm{B}T_\mathrm{v}, \end{aligned} \tag{6}$$

where

$$\delta = \frac{N}{N_\mathrm{c}}; \quad \varepsilon = \frac{P}{N_\mathrm{v}}, \tag{7}$$

and $E_{\mathrm{c}0}$ and $E_{\mathrm{v}0}$ are the energies of the CB and VB band edges respectively.

At the high carrier density levels usually presented in SOA P equals N. N_c and N_v are constants given by

$$N_\mathrm{c} = 2\left(\frac{m_\mathrm{e}kT}{2\pi\hbar^2}\right)^{\frac{3}{2}}; \quad N_\mathrm{v} = 2\left(\frac{m_\mathrm{dh}kT}{2\pi\hbar^2}\right)^{\frac{3}{2}}, \tag{8}$$

where

$$m_\mathrm{dh} = \left(m_\mathrm{hh}^{\frac{3}{2}} + m_\mathrm{lh}^{\frac{3}{2}}\right)^{\frac{2}{3}}, \tag{9}$$

m_e is the effective mass of electron in the CB. m_lh and m_hh are the effective mass of light hole and heavy hole in the VB.

The quasi-equilibrium values $\bar{n}_i(z,\tau)$ are given by:

$$\begin{aligned} &\bar{n}_\mathrm{c}(z,\tau) \\ &= N_0 F\left(E_\mathrm{fc}(z,\tau), T_\mathrm{c}(z,\tau), (E_{\mathrm{c}0} + E_\mathrm{c})\right), \end{aligned} \tag{10}$$

$$\begin{aligned} &\bar{n}_x(z,\tau) \\ &= f\bar{n}_y(z,\tau) \\ &= \frac{fN_0}{1+f}\left[1 - F\left(E_\mathrm{fv}(z,\tau), T_\mathrm{v}(z,\tau), (E_{\mathrm{v}0} - E_\mathrm{v})\right)\right], \end{aligned} \tag{11}$$

where f is the population imbalance factor describing the gain anisotropy introduced by tensile strain in the SOA.

The optical power $P^{\mathrm{TE/TM}}$ for each mode is related to the photon density $S^{\mathrm{TE/TM}}$ according to

$$S^{\mathrm{TE/TM}} = \frac{P^{\mathrm{TE/TM}}}{\hbar\omega_0}\frac{1}{v_\mathrm{g}WD}, \tag{12}$$

where W and D are the active region width and thickness of SOA respectively.

The transfer function of PC can be obtained in Ref.[14]. The overall transfer matrix of PC is given by

$$\begin{aligned} T &= Q(\theta+\xi)H(\gamma)Q(\theta) \\ &= \begin{pmatrix} A - \mathrm{j}B & -C - \mathrm{j}D \\ C - \mathrm{j}D & A + \mathrm{j}B \end{pmatrix} \end{aligned} \tag{13}$$

with

$$\begin{aligned} A &= -\cos\tilde{\gamma}\cos(\xi/2), \\ B &= -\sin\tilde{\gamma}\sin(\theta+\xi/2), \\ C &= -\cos\tilde{\gamma}\sin(\xi/2), \\ D &= \sin\tilde{\gamma}\cos(\theta+\xi/2), \\ \tilde{\gamma} &= \gamma - \theta - \xi/2. \end{aligned} \tag{14}$$

The matrix T describes general elliptical birefringence, where $\theta/2$ is the azimuth of the first quarter-wave plate (QWP), $\gamma/2$ is the azimuth of a half-wave

plate (HWP) and $(\theta+\xi)/2$ is the azimuth of the second QWP.

The intensity $S_{\rm out}^{\rm PBS}$ of the light that outputs the PBS is given by

$$S_{\rm out}^{\rm PBS} = S_{\rm PC}^{\rm TE} + S_{\rm PC}^{\rm TM} + 2\sqrt{S_{\rm PC}^{\rm TE} S_{\rm PC}^{\rm TM}}\cos\theta_{\rm PC}, \quad (15)$$

where $S_{\rm PC}^{\rm TE}$ and $S_{\rm PC}^{\rm TM}$ represent the intensities of the TE and TM components of the probe signal at the output of PC3 respectively and $\theta_{\rm pc}$ is the phase difference between the TE and TM modes of probe signal at the input of PBS.

The pulse spectrum is obtained by using

$$S(\omega) = \left|\int_{-\infty}^{\infty} [P(t)]^{1/2}\exp[{\rm i}\phi(t)+{\rm i}(\omega-\omega_{\rm c})t]{\rm d}t\right|^2, \quad (16)$$

where $P(t)$ and $\phi(t)$ are the pulse power and phase respectively and $\omega_{\rm c}$ is the central angular frequency of the pulse.

The filter in the system is modelled as a Gaussian filter with a full-width at half-maximum (FWHM) of 1.665 D. The transfer function of the filter is

$$f(\omega) = \sqrt{(1-\alpha_{\rm F})}\exp[-(\omega-\omega_{\rm f})^2/(2D^2)], \quad (17)$$

where $\omega_{\rm f}$ is the central angular frequency of the filter and $\alpha_{\rm F}$ is the insertion loss.

To evaluate the performance of the wavelength conversion scheme, the output ER is selected as the criteria, and it is defined as:

$${\rm ER} = 10\log\frac{P_{\rm out1,aver}}{P_{\rm out0,aver}}. \quad (18)$$

Here, $P_{\rm out1,aver}$ is the average power of the output probe pulses which are '1' levels, and $P_{\rm out0,aver}$ is the average power of the output probe pulses which are '0' levels.

3. Simulated results and discussions

The active volume of SOA is $50\,\mu{\rm m}^3$. The key parameters of the SOA used in simulation are listed in Table 1. Except for specially pointing out, the SOA is biased with a current of 280 mA. The pulse-width of pump and probe signals are 150 fs. The wavelength of pump and probe signals are 1545.9 nm and 1549.9 nm, respectively. The mean input pump power is 5 mW (7 dBm) and the mean input power of probe signal is 0.63 mW (−2 dBm). The pump and probe signals are

Table 1. SOA parameter definitions and their values.

parameter	symbol	value	units
active volume	$V = L\times W\times D$	$250\times 2\times 0.1$ [11]	$\mu{\rm m}^3$
confinement factor TE/TM	$\Gamma^{\rm TE}$, $\Gamma^{\rm TM}$, Γ_2	0.22, 0.17, 0.5	
phase modulation coefficients	α, α_2	5, −1.5	
FCA coefficients	$\beta_{\rm c}$, $\beta_{\rm v}$	3×10^{-8}, 0 [11]	$\mu{\rm m}^2$
internal loss	$\alpha_{\rm int}$	0.00175 [11]	$\mu{\rm m}^{-1}$
gain coefficient TE/TM	$a^{\rm TE}$, $a^{\rm TM}$	2.6×10^{-5}	$\mu{\rm m}^3$/ps
group velocity	$v_{\rm g}$	100 [11]	μm/ps
hole population imbalance factor	f	0.9 [11]	
electron-hole pair lifetime	$\tau_{\rm s}$	200	ps
optical transition energies (CB)	$E_{\rm c}$, $E_{2\rm c}$	0.03, 0.7 [11]	eV
optical transition energies (VB)	$E_{\rm v}$, $E_{2\rm v}$	0.003, 0.07 [11]	eV
carrier-carrier scattering times	$\tau_{1\rm c}$, $\tau_{1\rm v}$	0.1, 0.05 [15]	ps
carrier-phonon relaxation times	$\tau_{\rm hc}$, $\tau_{\rm hv}$	0.7, 0.25 [15]	ps
TPA coefficient	β_2	9×10^{-7} [11]	$\mu{\rm m}^2$
characteristic energies	$u_{\rm c}$, $u_{\rm v}$	0.145, 0.0431 [12]	eV
characteristic energies coefficient	$h_{\rm c}$, $h_{\rm v}$	6.26, 3.41 [12]	$10^{-21}m^3\cdot{\rm K/eV}$
optical transition state density	N_0	3.6×10^{6} [11]	$\mu{\rm m}^{-3}$
effective mass of electron in the CB	$m_{\rm e}$	4.10×10^{-32} [16]	kg
effective mass of heavy hole in the VB	$m_{\rm hh}$	4.19×10^{-31} [16]	kg
effective mass of light hole in the VB	$m_{\rm lh}$	5.06×10^{-32} [16]	kg

linearly polarized along 45° with respect to the polarization axes of TE and TM modes (noted as TE+TM) in wavelength conversion. For those parameter values, the initial values of gains for TE/TM modes are $0.187\,\mu\mathrm{m}^{-1}$ and $0.208\,\mu\mathrm{m}^{-1}$, corresponding to 17dB and 16.5 dB for small-signal amplification of the TE and TM modes, respectively.

3.1. Temporary characteristics

In Fig.2, the temporary gain and phase shift variations of TE probe signal induced by the different polarization modes of pump signal as a function of pump-probe time delay are presented. It can be seen from Fig.2 that the results are in good qualitative agreement with the experimental results presented in Ref.[17], where the gain and phase shift variations of probe signal induced by a fixed polarization mode of pump signal are presented. In Fig.2(a), the results show that the largest decrease in the TE gain takes place if the pump signal is also TE polarized, and the smallest decrease in the TE gain takes place if the pump signal is TM polarized. The phase shift variations of the TE probe signal induced by different polarization modes of pump signal are shown in Fig.2(b). The results show that the largest phase shift in the TE mode takes place if the pump signal is also TE polarized and the smallest phase shift in the TE mode takes place if the pump signal is TM polarized. Similar results hold for the gain and phase shift of TM probe signal. The reason for the trends is that the polarization selection rules inhibit stimulated transitions caused by the pump signal when the pump signal and probe signal are cross-polarized,[18] whereas the stimulated transitions increase the reduction of the carriers in SOA, which leads to reduce gain and increase the refractive index dynamic. The increase of the refractive index dynamic leads to increase the phase shift. Furthermore, it can be seen that the temporary gain of SOA induced by pump signal can recover after 1.5 ps, which indicates that it is possible that the wavelength conversion based on NPR can work at the rate of 640 Gbit/s.

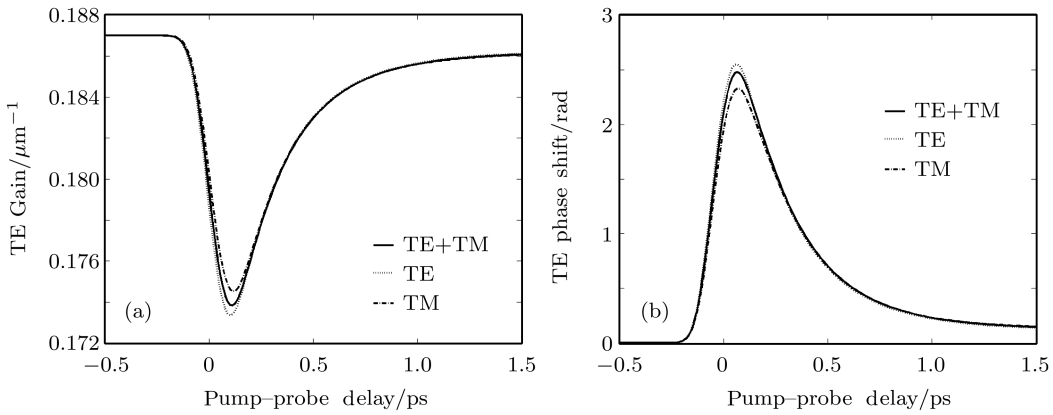


Fig.2. Temporary gain and phase shift of probe signal induced by different polarization modes of pump signal as a function of pump–probe time delay, where the pump signal is linearly polarized along the TE, the TM polarization axis or 45° with respect to the polarization axes of TE and TM modes (noted as TE+TM).

3.2. All-optical wavelength conversion based on NPR

The static operations of the wavelength conversion are presented in Fig.3. Static operation means that the pump signal is not modulated. In Fig.3, the output power of the probe signal from the PBS is plotted versus the power of the input pump signal for both of the inverted and the non-inverted cases. It can be seen from Fig.3 that ER of the converted signal can be over 20 dB. In this wavelength conversion scheme, because high-intensity pump light is used, NPR effect is expected, there is also XGM effect between pump and probe signals. Due to the presence of XGM effect, the non-inverted wavelength conversion caused by NPR is reduced, whereas the inverted wavelength conversion is enhanced. As a consequence, the slope of the curve for the inverted case (Fig.3(a)) is sharper than the one for the non-inverted case (Fig.3(b)). Moreover, it can be seen that the slope of the non-inverted transfer curve is larger than 1 when the input power of pump

signal is at the range from −10 dBm to 0 dBm, which indicates that the non-inverted wavelength conversion has the regeneration capability.

The simulated waveforms, eye diagrams and spectra at 640 Gbit/s for inverted and non-inverted wavelength conversions based on NPR are shown in Fig.4. The left hand is the inverted wavelength conversion case and the right hand is the non-inverted case. It can be seen that both of the non-inverted and inverted wavelength conversions based on NPR can work at 640 Gbit/s. In Fig.4, ultra-fast gain recovery is clearly visible at the SOA output, which in turn is followed by the slow gain recovery process driven by the inter-band carrier injection for the inverted wavelength conversion. It means that XGM is prominent in the inverted wavelength conversion. For the case of the non-inverted wavelength conversion, the output ER is about 10 dB and the eye diagrams are open although the variances for the '1' levels show that there is somewhat patterning effect.

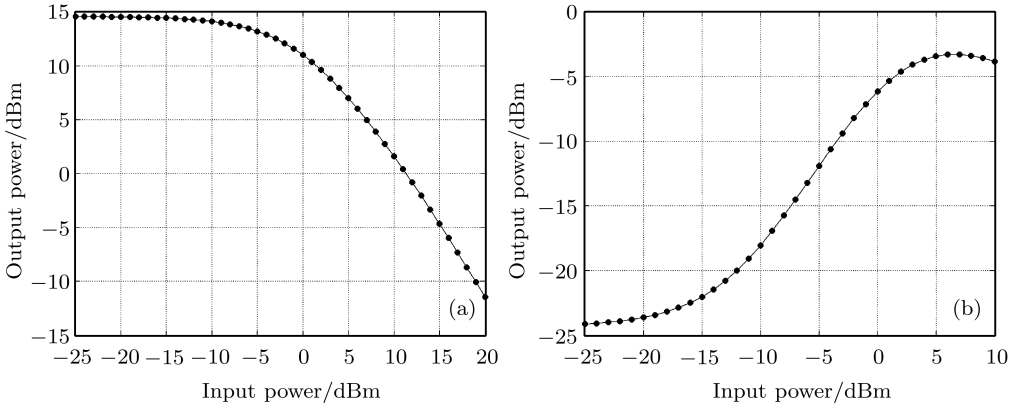


Fig.3. Static output power of probe signal versus the input power of pump signal. (a) Inverted wavelength conversion, (b) non-inverted wavelength conversion.

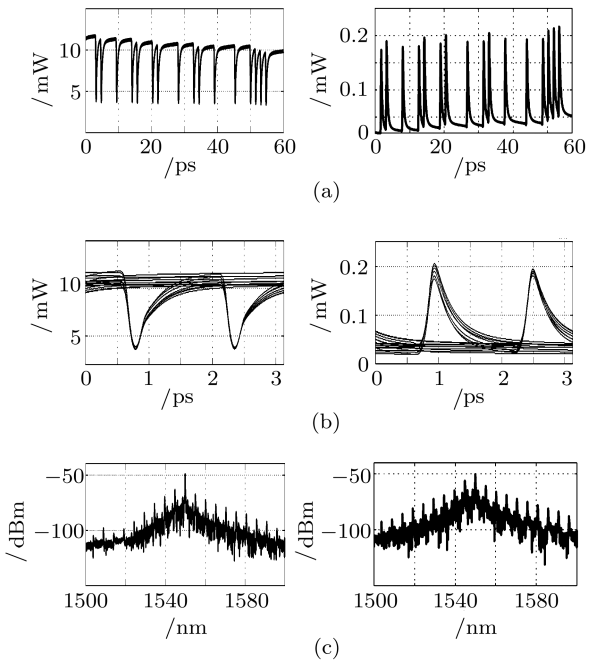


Fig.4. Waveforms, eye diagrams and spectra for inverted and non-inverted wavelength conversion output at 640 Gbit/s. (a) Waveforms, (b) eye diagrams, (c) spectra.

The discussions below are emphasized on the non-inverted wavelength conversion because this kind of wavelength conversion scheme is used widely in practice. In Fig.5(a), the dependence of output ER on the input pump signal power for 640 Gbit/s non-inverted wavelength conversion is presented. In Fig.5(a), the polarization of output probe signal from PC3 is vertical to the principal axis of PBS when only the probe signal is presented. With the increase of pump signal power, the polarization of output probe signal from PC3 is closing to the principal axis of PBS, which leads to the increase of the output ER. When the pump signal power reaches about 5 mW, the polarization of output probe signal from PC3 is deviating from the principal axis of PBS again, which leads that the output ER is decreasing with the increase of the power of pump signal. Then, the same variation trend takes place with the increase of the pump signal power.

Furthermore, it can be seen that the output ER of the non-inverted wavelength conversion for TE polarization mode of input pump signal is highest and for TM polarization mode of input pump signal is lowest under the same conditions from Fig.5(a). To further prove it, the dependence of output ER of non-inverted

wavelength conversion on the polarization angle of input pump signal is presented in Fig.5(b). The polarization angle of input pump signal is defined as the angle between the polarization orientation of input pump signal and the TE polarization orientation. It can be seen that the maximum output ER can be achieved when the input pump signal is TE mode and the minimum output ER is obtained when the input pump signal is TM mode, which agree well with Fig.5(a). The maximum output ER is above 13dB and the minimum output ER is about 5dB. The reason is that the gain variation and the phase shift of probe signal induced by TE polarization mode of input pump signal are largest, which are favourable for the improvement of output ER of the non-inverted wavelength conversion based on NPR.

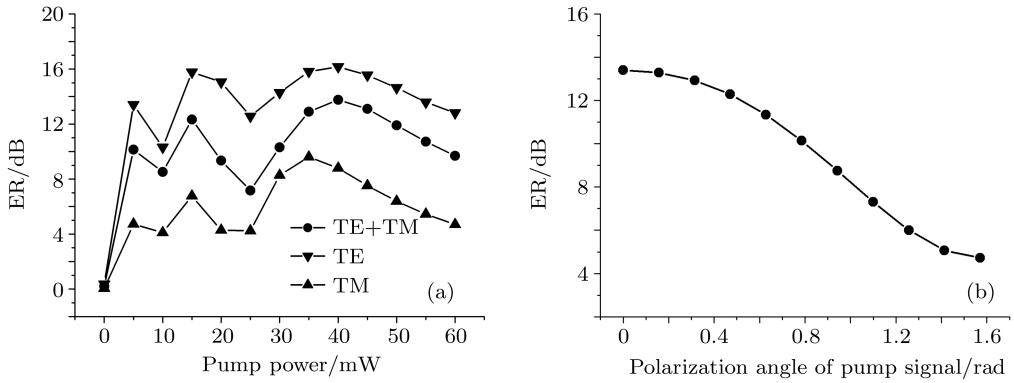


Fig.5. Dependence of output ER on key parameters for 640 Gbit/s non-inverted wavelength conversion. (a) Input pump signal power, (b) polarization angle of input pump signal.

3.3. All-optical wavelength conversion based on NPR assisted with red-shifted filtering

The configuration of non-inverted all-optical wavelength conversion based on NPR assisted with red-shifted filtering is illustrated in Fig.6. The principle of the wavelength conversion scheme is the same

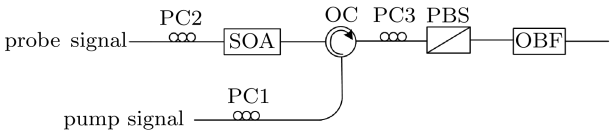


Fig.6. Principle of non-inverted all-optical wavelength conversion based on NPR assisted with red-shifted filtering. OBF: optical band-pass filter.

as that of the wavelength conversion only based on NPR except that the output signal from PBS is red-shifted filtered by an OBF. The simulated waveforms, eye diagrams and spectra at 640 Gbit/s non-inverted conversion are shown in Fig.7. In this figure, the right sides are the simulated results for non-inverted wavelength conversion based on NPR assisted with red-shifted filtering. For comparison, the results for non-inverted wavelength conversion only based on NPR

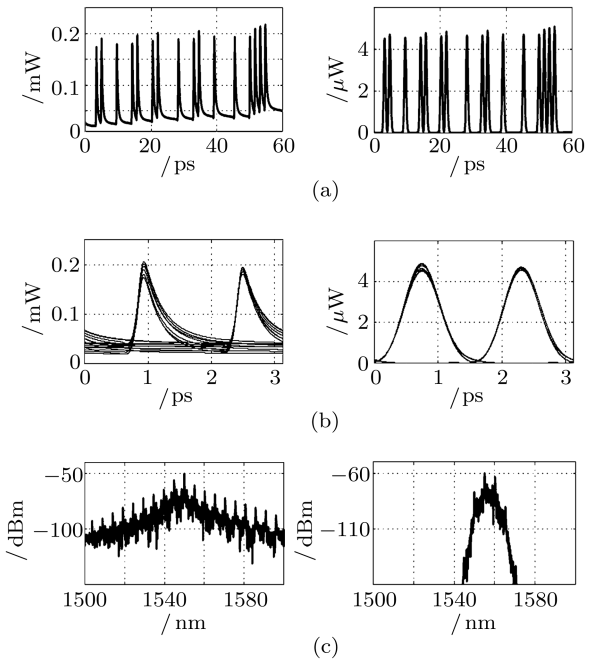


Fig.7. Waveforms, eye diagrams and spectra for the output of wavelength conversions based on NPR and NPR assisted with red-shifted filtering at 640 Gbit/s. (a) Waveforms, (b) eye diagrams, (c) spectra.

are also shown in the left sides of this figure. The wavelength and bandwidth of the filter are 1556 nm and 5 nm respectively. It can be seen that for wave-

length conversion only based on NPR the eye diagrams of the converted wavelength signal are asymmetric due to the slow gain recovery time of SOA. In contrast, in case of wavelength conversion based on NPR assisted with red-shifted filtering, there are a high ER and clear open and very symmetric eye diagrams although the output pulses are somewhat broadened. The ER of the two kinds of non-inverted wavelength conversion schemes are 10 dB and 16 dB respectively, which shows that the performance of the non-inverted wavelength conversion based on NPR can be improved by using a red-shifted filtering scheme.

4. Conclusion

In this paper, we develop a model of wavelength conversion based on NPR, which accounts for ultrafast carrier dynamics. In this model, we introduce two carrier temperature equations to substitute two energy density equations, which reduce the complexity of calculation.

By the analyses on the temporary characteristics of SOA induced by ultra-short pulses, we can see that the largest decrease in gain and the largest phase shift of probe signal will take place if the pump signal is the same polarization as the probe signal.

Simulated results show that the 640 Gbit/s non-inverted and inverted wavelength conversions based on NPR can be achieved with open eye diagrams. The output ER of the non-inverted wavelength conversion can be reached 10 dB. Moreover, the non-inverted wavelength conversion scheme can be used to achieve regeneration function by the analyses on the static operations of the wavelength conversion based on NPR.

By the discussions on the performance of the non-inverted wavelength conversion, we can see that the output ER of non-inverted wavelength conversion is sensitive to input pump power, which should be optimized according to the practical application. For different polarization modes of input pump signal, the output ER of non-inverted wavelength conversion with TE mode input pump signal is higher than that of the wavelength conversion with other mode input pump signal.

Furthermore, we present a high performance wavelength conversion scheme based on NPR assisted with red-shifted filtering. The output ER of the wavelength conversion scheme is higher 6 dB than that of the wavelength conversion scheme only based on NPR under the same conditions.

References

[1] Zhang X L, Huang D X, Sun J Q and Liu D M 2001 *Chin. Phys.* **10** 124

[2] Li P L, Huang D X, Zhang X L and Zhu G X 2006 *Acta Phys. Sin.* **55** 2746 (in Chinese)

[3] Asghari M, White I H and Penty R V 1997 *IEEE J. Lightwave Technol.* **15** 1181

[4] Contestabile G, Presi M and Ciaramella E 2004 *IEEE Photon. Technol. Lett.* **16** 1775

[5] Nesset D, Kelly T and Marcenac D 1998 *IEEE Commun. Mag.* **36** 56

[6] Ellis A D, Kelly A E, Nesset D, Pitcher D, Moodie D G and Kashyap R 1998 *Electron. Lett.* **34** 1958

[7] Wei C C, Huang M F and Chen J 2005 *IEEE Photon. Technol. Lett.* **17** 1683

[8] Liu Y, Hill M T, Tangdiongga E, de Waardt H, Calabretta N, Khoe G D and Dorren H J S 2003 *IEEE Photon. Technol. Lett.* **15** 90

[9] Turkiewicz J P, Khoe G D and de Waart H 2005 *Electron. Lett.* **41** 29

[10] Cotter D, Manning R J, Blow K J, Ellis A D, Kelly A E, Nesset D, Phillips I D, Poustie A J and Rogers D C 1999 *Science* **286** 1523

[11] Yang X, Lenstra D, Khoe G D and Dorren H J S 2003 *Opt. Commun.* **223** 169

[12] Uskov A, Mork J and Mark J 1992 *IEEE Photon. Technol. Lett.* **4** 443

[13] Nilsson N G 1978 *Appl. Phys. Lett.* **33** 653

[14] Heismann F 1994 *IEEE J. Lightwave Technol.* **12** 690

[15] Mork J and Mark J 1994 *Appl. Phys. Lett.* **64** 2206

[16] Connelly M J 2001 *IEEE J. Quant. Electron.* **37** 439

[17] Hultgren C T, Dougherty D J and Ippen E P 1992 *Appl. Phys. Lett.* **61** 2767

[18] Hall K L, Darwish A M, Ippen E P, Koren U and Raybon G 1993 *Appl. Phys. Lett.* **62** 1320